

SOLAR CELLS FROM 120 PPMA CARBON-CONTAMINATED FEEDSTOCK WITHOUT SIGNIFICANTLY HIGHER REVERSE CURRENT OR SHUNT

P. Manshanden and G. Coletti
 ECN Solar Energy, P.O. Box 1, 1755 ZG Petten, The Netherlands,
 Phone: +31 88 515 4765, Fax: +31 88 515 8214, E-mail: manshanden@ecn.nl

ABSTRACT: In a bid to drive down the cost of silicon wafers, several options for solar grade silicon feedstock have been investigated over the years. All methods have in common that the resulting silicon contains higher levels of impurities like dopants, oxygen, carbon or transition metals, the type and level of impurities depending on the raw materials and refining processes. In this work wafers from a p-type mc-Si ingot made with feedstock contaminated with 120 ppma of carbon have been processed into solar cells together with reference uncontaminated feedstock from semiconductor grade polysilicon with <0.4 ppma carbon. The results show that comparable reverse current, shunts, and efficiencies can be reached for both types of wafers. Gettering and defect hydrogenation effectiveness also did not deviate from the reference. Electroluminescence pictures do not show increased hotspot formation, even at -16V.

Keywords: solar grade silicon, carbon, multicrystalline silicon, feedstock

1 INTRODUCTION

In a bid to drive down the cost of silicon wafers, several options for solar grade silicon feedstock have been investigated over the years, e.g. Solsilc [1] or Photosil [2]. A common property of solar grade silicon feedstock is higher concentrations of impurities [3] like oxygen, carbon, dopants or transition levels. In this paper we focus on the impact of carbon on solar cell characteristics.

Carbon as a dissolved impurity in silicon only causes few problems, because it occupies a substitutional place in the lattice and is electrically neutral [4]. It is known to have effect on other impurities however, most notably oxygen[5] in the form of enhanced oxygen clustering. Above the solid solubility level, carbon precipitates as silicon carbides, which are a source of dislocations formation [6]. Silicon carbides are also good conductors, and as they grow preferentially along the solidification front, they tend to contact the two polarities of a solar cell, leading to severe shunting [7]. Moreover, silicon carbides present a severe risk for wire sawing because of the hardness of the precipitates; 9-9.5 on the Mohs scale *versus* 7 for silicon.

Because substitutional carbon is of little influence on cell performance in contrast to the carbides, the solubility of carbon at the melting point of silicon is taken as maximum allowed carbon level in ingots, which is 9 ppma.

The goal of the investigation presented in this paper is to show that good cells can be obtained from high carbon feedstock by controlling carbon precipitation during crystallisation.

2 EXPERIMENTAL

2.1 Ingot and wafer selection

Ingots were grown by directional solidification with feedstock contaminated with 120 ppma carbon (ingot A), as well as with reference feedstock (ingot B) with less than 0.4 ppma carbon, which is below the detection limit of the analytical method used. Carbon precipitates were noticed in the slug of the ingot surface for ingot A. From both ingots five bricks were selected, two from the centre, one from the edge and two from the corner of the ingot. Both ingots were sawn with a wire saw without

any issue yielding approximately 500 wafers from each brick.

From the first set of corner and centre bricks and the edge bricks wafers were selected homogeneously throughout the brick (bottom to top) for each ingot. From the other corner and centre bricks 40 wafers were processed from the extreme top and bottom of the brick to provide some statistics on the parts of the ingots which normally contain the highest concentration of impurities.

2.2 Wafer characterization process

The wafers for characterization consisted of a set of 3 neighbour wafers per position. Each neighbour set was distributed to a different group: an as-grown group, a gettered group and a gettered and passivated group in order to study the effect of the high carbon concentration on the gettering and passivation processes. The applied processing is shown in Table I.

Table I: wafer characterization groups

	As grown	Gettered	Gettered + passivated
Acid texture	x	x	x
P-diffusion		x	x
PECVD SiN _x			x
SiN _x removal			x
Emitter removal		x	x

After the process as shown in Table I, the wafers were subsequently chemically polished and the interstitial oxygen and substitutional carbon concentration was measured by FTIR using SEMI MF1188 and SEMI MF 1391. Deviation from the standards by using a wafer thickness thinner than described was unavoidable, as the maximum thickness of wafers is thinner than the minimum thickness SEMI prescribes. As we have shown before [8], we can incorporate this deviation by using an uncertainty estimate of 1.3 ppma.

The polished wafers were then passivated with passivating PECVD SiN_x, which yields an approximate surface passivation S of 10-20 cm/s. Then the minority carrier lifetime of the wafers was measured by QSSPC.

2.2 Solar cell process

Neighbour wafers from the wafer characterization process, as well as the 40 wafers from top and bottom,

were processed into solar cells using a H-pattern Al-BSF $\text{Si}_3\text{N}_4\text{:H}$ firing through cell process. The process flow of this baseline process is shown in Figure 1.

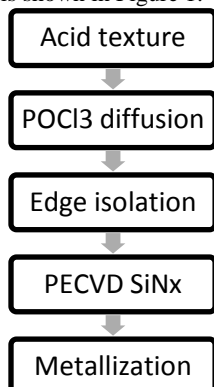


Figure 1: ECN solar cell baseline process flow

The solar cells' IV characteristics were measured with a WACOM solar simulator class AAA under STC according to IEC 60904. Shunts were localized using the ECN homebuilt electroluminescence (EL) setup.

3 RESULTS

3.1 Carbon contents

The carbon concentration of the wafers is shown in Figure 2.

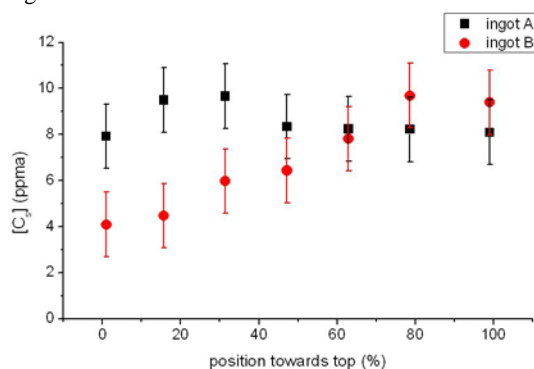


Figure 2: substitutional carbon concentration through the ingot height

The substitutional carbon content through the ingot is almost constant within the uncertainty for ingot A which was made of high carbon feedstock, and followed a typical segregation curve for the reference ingot B within the uncertainty.

The interstitial oxygen concentration ranged from 4 ppma at the bottom of the ingots to 2 ppma at the top for both ingots.

The resistivity curve of the two ingots overlaps and ranges from 1.6 Ohm cm at the bottom of the ingot to 1.2 Ohm cm at the top of the ingot.

3.2 Minority carrier lifetime

Using the process flow of Table I, we tracked the gettering and hydrogenation efficacy on the wafers from the two ingots to see if the enhanced carbon content had any influence on the gettering and hydrogenation behaviour.

Gettering efficacy can be expressed as the ratio initially present interstitial iron and of interstitial iron

gettered by the process. This is depicted in Figure 3.

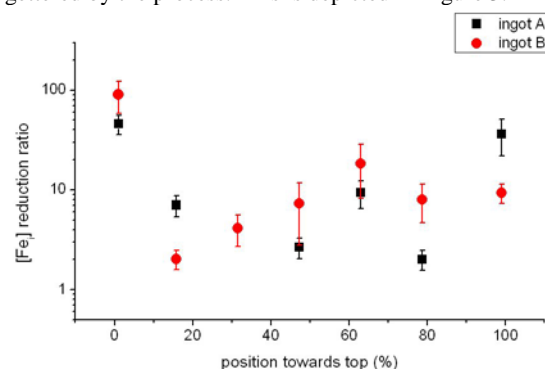


Figure 3: ratio of interstitial iron gettered by POCl_3 diffusion

Because the associated errors with low $[\text{Fe}_i]$ are much larger, the errors are larger in the centre of the ingot, where the $[\text{Fe}_i] \approx 10^{11} \text{ cm}^{-3}$. As the ratio of gettered interstitial iron is approximately equal for both ingots, taking into account that the top and bottom of the ingot are actually the top and bottom of the portion used for cells, we can conclude that carbon does not impede gettering efficiency of iron.

The results of the final process step are depicted in Figure 4. Note that data of ingot A is sometimes obscured by the data points of ingot B because of overlap.

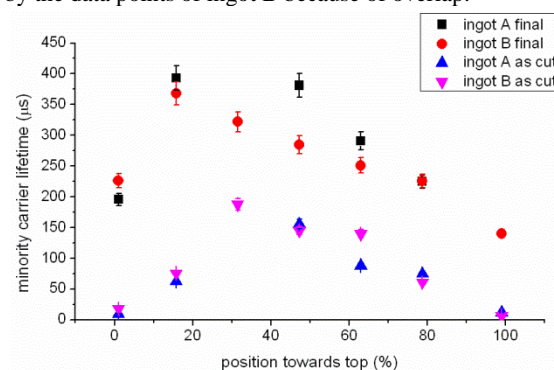


Figure 4: minority carrier lifetime as cut and after gettering and hydrogenation

Figure 3 and Figure 4 together show that ingot A is with respect to gettering and hydrogenation effects virtually undistinguishable from ingot B on wafer level.

3.3 Precipitate detection.

If silicon carbide particles are present, they are expected to stick out of the grain boundaries, perpendicular to the cell surface. Investigation of these particles has been carried out on etched samples under optical microscope, but none have been found.

3.4 Cell efficiencies

As the wafers have identical resistivity, cells should be able to reach comparable J_{sc} and V_{oc} with identical processing – provided the minority carrier lifetimes after processing (Fig. 4) are comparable. After IV measurement, this prediction proved to be accurate. Therefore, the efficiency gives an accurate indication of the forward bias behaviour of current and voltage (see Figure 5).

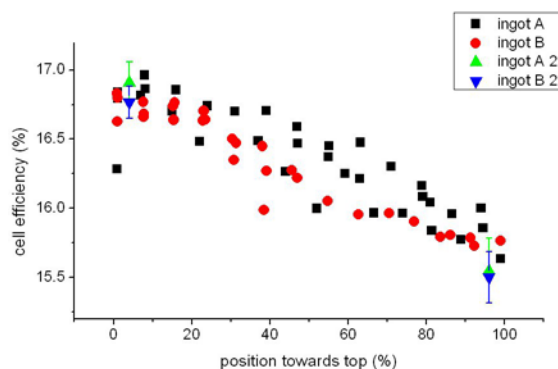


Figure 5: efficiency throughout the ingot of ingot A and B. Ingot A2 and Ingot B2 are the average of 2 times 40 neighbouring cells

3.5 Shunt and reverse current

Shunt values of both ingots from a single diode fit are depicted in Figure 6. As cells are considered shunted below 10 Ohm shunt resistance, the cells of interest are the ones closest to zero. In order to make the cells of interest stand out, the unit used in Figure 6 is the inverse of resistance; the shunt conductance.

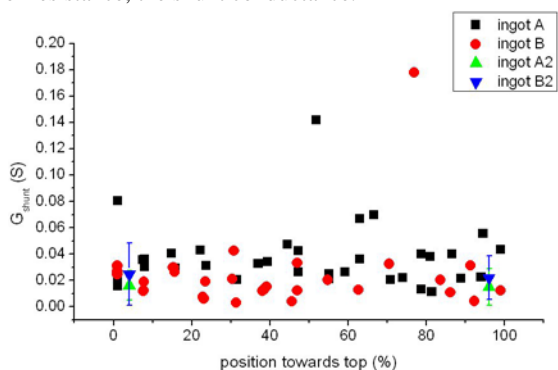


Figure 6: shunt conductance of the cells throughout ingot A and B. Ingot A2 and B2 refer to the two neighboursets from different bricks.

A solar cell is considered 'shunted' if the shunt conductance is as high as 0.10 S which equals 10 Ohms shunt resistance. One cell from ingot A and one cell from ingot B prove to be shunted which was due to wafer cracks. Carbon precipitate shunting is expected to show especially in the top of the ingot. This is not observed from our data.

If inclusions present a diode-like behaviour, the cells are not shunted but they do have reverse current problems. The reverse current of the cells is shown in Figure 7.

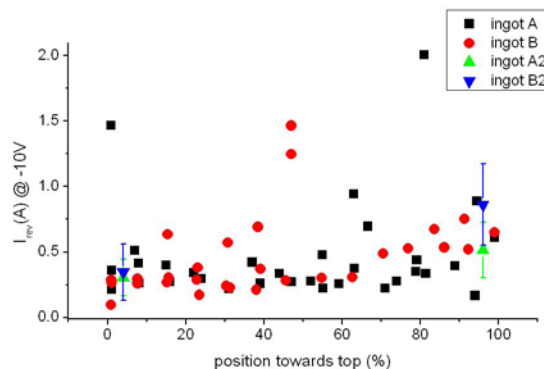


Figure 7: reverse current at -10 V for the two ingots and averages

Rather arbitrarily it was decided that reverse current values of less than 1 A at 10 V is sufficient. Four cells do not fulfil this criterium; two of ingot A and two of ingot B. However, all four cells have the reverse current identified as edge shunts, cracks or other processing defects. Also, the average of ingot B (blue triangle) with its standard deviation is close to that limit, much closer than the average of ingot A.

For a number of cells of ingot A the reverse IV characteristic was recorded to see if any late onset (>-10V) breakdown problems would occur (see Figure 8). The used cells are included in Figure 7, but are not affected by processing faults.

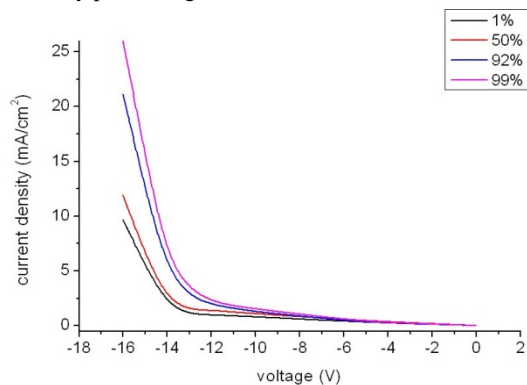


Figure 8: reverse IV characteristic of cells at different height towards top of ingot A

The cells show type III breakdown effects, as classified by Breitenstein *et al.* [9], or avalanche breakdown. The fact that it occurs a bit sooner for the top wafers is as expected, and has been observed on several occasions. [9,10] The current density at -16 V for the topmost wafer is still acceptable for module manufacturing.

3.6 Electroluminescence images

EL images from the top and bottom of the ingot were taken at -16 V (see Figure 9).

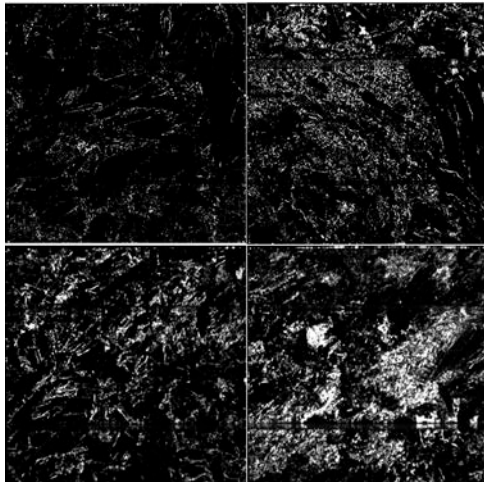


Figure 9: EL picture at -16 V for bottom (upper left) and top (upper right) cells of ingot A, and for bottom (lower left) and top (lower right) cells of ingot B, all at the same scale

The increase in luminescence corresponds to an increase in current density (see Fig. 8). Important for module manufacturing is that the current is dissipated fairly homogeneously over the entire cell, avoiding hot spot formation.

The increase in luminescence between ingot A and B is translated in an increase in reverse current. The level of reverse current for ingot B should still be acceptable for module manufacturing. This is simply due to accidental variations in ingot growth which occurs between any two ingots.

4 CONCLUSIONS

An ingot grown with 120 ppma carbon containing feedstock has been investigated to study the impact of carbon on solar cell performance. Literature shows that carbon precipitates should be evident as shunts, or perhaps reverse currents, and it can also be found as a distinct particle sticking out of an etched sample. No evidence of silicon carbides in the ingot has been found. In addition the solar cell performance are comparable to that one of reference ingot without carbon contamination. Reverse current and shunts resistance are also comparable with reference material.

5 REFERENCES

- [1] R.Kvande *et al.* 25th EUPVSC (2010) pg 1220
- [2] J.Kraiem *et al.* Proceedings 35th IEEE PVSC (2010) no. 326
- [3] SEMI PV17-0312 - Specification for Virgin Silicon Feedstock Materials for Photovoltaic Applications
- [4] R.C. Newman, Rep. Prog. Phys., Vol. 45 (1982)
- [5] H.J. Möller *et al.*, Solid State Phenomena Vols. 156-158 (2010) pp 35-40
- [6] S. Pizzini *et al.*, J. Electrochem. Soc. 135 (1988) 155.
- [7] J. Bauer *et al.*, 21st EUPVSC (2006) pg 1115
- [8] P. Manshanden *et al.* 24th EUPVSC (2009) pg 1148
- [9] O. Breitenstein *et al.* JAP 109, 071101 (2011)
- [10] D. Lausch *et al.*, Phys. Status Solidi 3, 70 (2009).